

Analytical model for the thermal conductance of double-compound honeycomb transparent insulation, with validation

J.E.Y. Hum, K.G.T. Hollands *, J.L. Wright

Department of Mechanical, Engineering University of Waterloo, Waterloo, Ont., Canada N2L 3G1

Received 17 February 2003; accepted 18 July 2003

Abstract

Whereas early thermal models of honeycomb transparent insulation assumed the honeycomb to be bounded by opaque plates on both faces, more recent models have allowed for an air gap between the honeycomb and one of the plates: the “compound honeycomb” configuration. This paper deals with a new configuration, one that is basically the compound honeycomb configuration, but the other bounding plate is diathermous (i.e., partly transparent to long-wave radiation) rather than opaque. This new configuration has arisen in the application of honeycombs in greenhouses. This paper extends the existing compound honeycomb model, by adding a new variable and a new equation. It was found that a 9×9 matrix needs to be inverted rather than the 8×8 required by the earlier formalism. To test the model, the overall conductance across a set of transparent honeycombs resting on one of two diathermous plastics was measured, using a guarded heater plate apparatus. The honeycombs were fabricated from UV-stabilized polypropylene, and had a cell size of about 10 mm. Although the model tended to slightly over-predict the measurements (by about 10%) it is considered to be accurate enough for design purposes.

© 2003 Elsevier Ltd. All rights reserved.

1. Introduction

Honeycomb transparent insulation has found application in building insulation, in skylights, as well as in solar collectors. A recent review of this and other transparent insulations has been given by Hollands et al. (2001). Heat transfer takes place through the honeycomb by the coupled modes of radiation and conduction. (The honeycomb cell size is normally small enough to eliminate any convective heat transfer.) Modeling the thermal conductance of honeycombs formed the subject of many early studies, in which the honeycomb was assumed to be bounded solid opaque plates adjacent to both faces. Hollands and Iynkaran (1984) suggested

leaving an air-gap between one bounding surface and the adjacent honeycomb face, forming what has come to be known as the “compound honeycomb”. (The purpose of the air gap is to de-couple the radiative and conductive modes near a low emissivity plate.) Platzer (1992), Hollands and Iynkaran (1993) and Arulanantham and Kaushika (1996) have presented more recent thermal-conductance models.

Recently a new configuration has arisen in which one of the bounding plates is not opaque, but is partly transparent to long-wave radiation, and the purpose of this paper is to describe a new thermal model aimed at treating this new configuration. The configuration has arisen from the use of honeycombs as an energy conservation measure in greenhouses. Here the honeycomb rests on a horizontal plastic sheet that is partly transparent to long-wave radiation, as in Fig. 1a. Below the plastic sheet is the main part of the greenhouse where the plants are grown. Above the honeycomb is the glass gable-roof of the greenhouse.

* Corresponding author. Tel.: +1-519-888-4043; fax: +1-519-888-6197.

E-mail addresses: kholland@mecheng1.uwaterloo.ca, kholland@solar1.uwaterloo.ca (K.G.T. Hollands).

Nomenclature

D	equivalent diameter for a honeycomb cell [m]
h_r	$h_r = \varepsilon_p \sigma (T_h^4 - T_c^4) (T_h - T_c)^{-1}$
h_t	overall heat transfer coefficient from hot plate to cold plate [$\text{W m}^{-2} \text{K}^{-1}$]
P	$P = (W_1 + b^2)^{1/2}$
R	$R = D/2$ [m]
t	equivalent thickness of honeycomb cell “demi-wall” [m]
W_1	$W_1 = 4\varepsilon_w \sigma D (T_h^4 - T_c^4) k_e^{-1} (T_h - T_c)^{-1}$
W_2	$W_2 = W_1 \varepsilon_p \varepsilon_w^{-1}$
W'	$W' = W_1 t D^{-1}$
Y_x	$(x = c, h, p), Y_x = T_x^4 (T_h^4 - T_c^4)^{-1}$

Greek symbols

κ	$\kappa = \rho_p (c - \lambda) c^{-1}$
λ	$\lambda = 1 - \exp(-2b\mu)$
$\varphi_1, \varphi_2, \varphi_3$	$\varphi_1 = \exp(P\mu), \varphi_2 = \exp(-P\mu), \varphi_3 = \varphi_1 - \varphi_2$
μ	$\mu = 0.5LD^{-1}$
v_1, v_2	$v_1 = \mu + b^{-1}, v_2 = -\mu + b^{-1}$
σ	Stefan–Boltzmann’s constant
ω_1, ω_2	$\omega_1 = b(P + b)^{-1}, \omega_2 = b(P - b)^{-1}$
$\Omega_1, \Omega_2, \Omega_3$	$\Omega_1 = (1 - \varepsilon_h) c^{-1}, \Omega_2 = (1 - \varepsilon_c) c^{-1}, \Omega_3 = \rho_p c^{-1}$

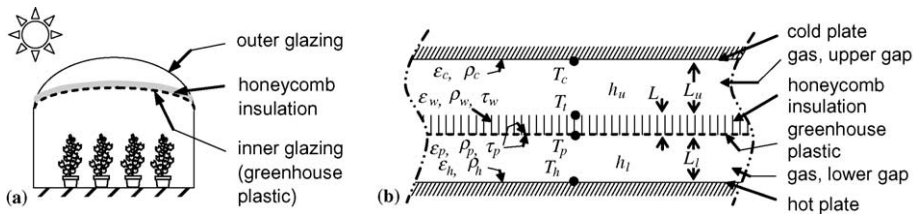


Fig. 1. (a) Typical greenhouse configuration with honeycomb insulation; (b) double-compound honeycomb configuration used to model the greenhouse situation in (a).

A model for this situation, as analyzed, is shown in Fig. 1b. The partly transparent sheet is called here the “greenhouse plastic”, although the application of model is not restricted to greenhouses. When, as we have here, the bounding plate is not opaque, the radiant properties of the plate below it are also important, and one must predict the overall thermal conductance from this lower plate (the hot plate in Fig. 1b) to the upper plate (the cold plate in Fig. 1b). Equations for the convective coefficients adjacent to the hot and cold plates are assumed to be known. The procedure adopted for treating the situation in Fig. 1b was to extend the Hollands and Iynkaran (1993) analytical model by adding three new variable—the temperature of the greenhouse plastic and the radiositivities on both sides—and three new equations. After some relatively simple substitutions, this system is reduced to 9 linear equations in 9 unknowns, and so a 9×9 matrix needs to be inverted to complete the solution (in contrast to the 8×8 matrix inversion required in the previous model).

To test the model, the overall conductance across a set of transparent honeycombs resting on one of two greenhouse plastics was measured, using a guarded heat plate apparatus. The measured overall thermal conductances ranged from 2.2 to 3.1 $\text{W m}^{-2} \text{K}^{-1}$. The model

tended to slightly over-predict the measurements, the difference being attributed to unavoidable edge effects in the measurements and also the grey, specular assumptions in the model.

2. Modeling and analysis

2.1. Greenhouse model

As has been mentioned, the greenhouse shown in Fig. 1a was modeled as shown in Fig. 1b. The influence of the solar radiation can be shown to be very small and is not included in the analyses. The infinite hot plate at temperature T_h and emissivity ε_h , represents the inside of the main greenhouse enclosure (plants, etc.), which will have a relatively high emissivity, close to unity. Above and parallel to it is the infinite cold plate at temperature T_c and emissivity ε_c , representing the greenhouse roof, which will also have an emissivity close to unity. These hot and cold bounding plates are assumed to be diffusely emitting and diffusely reflecting surfaces, which is considered appropriate for the greenhouse application. The honeycomb insulation, of depth L , rests on the sheet of greenhouse plastic, in the space between the hot and

cold plates. Above and below the honeycomb are the air gaps of heights L_u and L_l respectively, which are in free convective motion. These layers are characterized by convective heat transfer coefficients h_l and h_u in the lower and upper gaps, respectively. Also playing important roles are the long-wave radiant properties of the greenhouse plastic, which are its emissivity, ϵ_p , reflectance, ρ_p and transmittance, τ_p .

2.2. Honeycomb model

The honeycomb model of Hollands and Iynkaran (1993) contained many simplifications and assumptions which they justify on the basis of physical arguments and the fact that the model predictions fit experimental results. Except where noted, the same assumptions are made here, without further justification. Thus the analysis is based on a single circular honeycomb cell (Fig. 2) having adiabatic, opaque, specularly reflecting, gray, diffusely emitting (with emissivity ϵ_w), thin side-walls that have thickness equal to one-half the actual cell-wall thickness. The equivalent specular reflectance ρ^s of the honeycomb’s cell-wall is set equal to the sum of the reflectance and transmittance of a sample of the plastic sheet from which the honeycomb is fabricated; it is therefore equal to $1 - \epsilon_w$. Also, the air temperature inside this idealized honeycomb cylindrical cell is a function only of the axial co-ordinate z , and not of the radial co-ordinate. It is further assumed that $T_h/T_c \approx 1$, where T_h and T_c are absolute temperatures.

In contrast to Hollands and Iynkaran, who extended the cell-walls surfaces on *one* side by hypothetical adiabatic surfaces of 100% specular reflectivity, the cell-walls in the present study are extended both top and bottom

by similar hypothetical specular adiabatic surfaces, as shown in Fig. 2. This is to accommodate the presence of air volumes above and below the honeycomb in the greenhouse situation.

2.3. Governing equations and their solution

The model is broken into three regions as shown in Fig. 2: (i) the cell itself, for which $-L/2 \leq z \leq L/2$; (ii) the upper gap, for which $L/2 \leq z \leq L/2 + L_u$; and (iii) the lower gap, for which $-(L/2 + L_l) \leq z \leq -L/2$. The governing equations are similar to those of Hollands and Iynkaran (1993), but altered and extended to incorporate the greenhouse plastic. They are written in terms of the five temperatures T_i and the five diffuse radiosities J_i , with $i = w, h, c, p, pu$ and pl as follows: for the cell side-wall, $i = w$; for the hot plate, $i = h$; for the cold plate, $i = c$; for the temperature of the greenhouse plastic, $i = p$; for the radiosity of the upper side of the greenhouse plastic, $i = pu$, and for the radiosity of the lower side of the greenhouse plastic $i = pl$. Also included in the governing equations are the specular view factors F_{i-j} , in which i and j are indices that can take on any of w, h, c, pu and pl also, when either i or j is dw , the reference here is to an elemental ring of height dz on the cylinder, and when either i or j is dw' , the reference is to an elemental ring of height dz' on the cylinder. Other symbols are defined in the nomenclature. The first five governing equations are radiant balances each of the five surfaces, as follows:

$$J_w(z) = \epsilon_w \sigma T_w^4(z) \tag{1}$$

$$J_h = \epsilon_h \sigma T_h^4 + (1 - \epsilon_h)(J_{pl}F_{h-pl}) \tag{2}$$

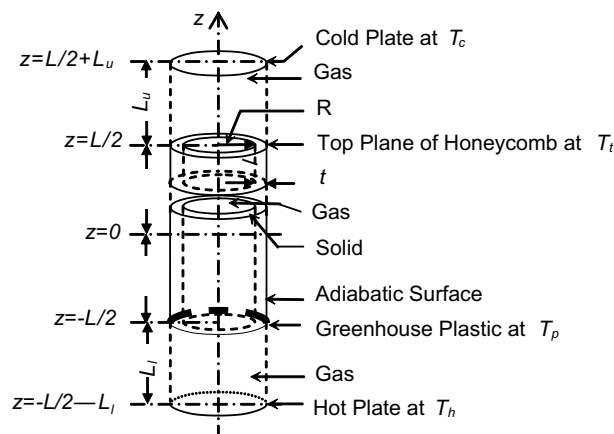


Fig. 2. Model of double-compound honeycomb cell.

$$J_c = \varepsilon_c \sigma T_c^4 + (1 - \varepsilon_c)(J_{pu} F_{c-pu} + \bar{J}_{w,c} F_{c-w}) \quad (3)$$

$$J_{pu} = \varepsilon_p \sigma T_p^4 + \tau_p J_h + \rho_p (J_c F_{pu-c} + \bar{J}_{w,pu} F_{pu-w}) \quad (4)$$

$$J_{pl} = \varepsilon_p \sigma T_p^4 + \rho_p J_h + \tau_p (J_c F_{pu-c} + \bar{J}_{w,pu} F_{pu-w}) \quad (5)$$

where

$$\bar{J}_{w,i} = \frac{1}{F_{i-w}} \int_{-L/2}^{+L/2} J_w(z') \frac{dF_{i-dw'}(z')}{dz'} dz' \quad (6)$$

Next, an expression for the energy balance at the wall is derived by equating the net energy radiated out of the interface with the net energy conducted into the interface. After some re-arrangement, this gives

$$\begin{aligned} \sigma T_w^4(z) - J_{pl} F_{w-p}(z) - J_c F_{w-c}(z) - \bar{J}_{w,w}(z) F_{w-w} \\ = \frac{k_c (R + t)^2}{2\varepsilon_w R} \frac{dT_w}{dz^2} \end{aligned} \quad (7)$$

where k_c is an effective thermal conductivity along the honeycomb cell, defined in the same way as by Hollands and Iynkaran, and

$$\bar{J}_{w,w}(z) = \frac{1}{F_{w-w}} \int_{-L/2}^{+L/2} J_w(z') \frac{dF_{dw-dw'}(z, z')}{dz'} dz' \quad (8)$$

An energy balance on the greenhouse plastic sheet gives

$$\begin{aligned} \varepsilon_p (2\sigma T_p^4 - J_h F_{p-h} - J_c F_{p-c} - \bar{J}_{w,w} F_{p-w}) \\ = k_c \left(\frac{dT_w(z)}{dz} \right)_{z=(-L/2)} + h_1 (T_h - T_p) \end{aligned} \quad (9)$$

where h_1 is the convective heat transfer coefficient across the lower gap.

The layer of thickness L_u between the top of the honeycomb and the cold plate contains convecting air. We can conceptually replace this air with a stationary gas layer of the same thickness, offering the same thermal resistance. Making the thermal resistance the same is achieved by giving the gas layer an apparent thermal conductivity k_g (different from the conductivity of air), so as to give the appropriate thermal resistance, as explained later; thus $k_g = h_u L_u$. With this replacement, the third energy balance, written at the plane $z = L/2$ gives

$$k_g \left(\frac{dT_g(z)}{dz} \right)_{z=L/2} = k_c \left(\frac{dT_w(z)}{dz} \right)_{z=L/2} \quad (10)$$

where $T_g(z)$ is the temperature distribution in the hypothetical upper layer, which, since the upper layer is stationary, must satisfy

$$\frac{dT_g^2(z)}{dz^2} = 0 \quad (11)$$

In addition to these equations we must have certain boundary conditions satisfied, principally $T_g(L/2) = T_w(L/2)$ and $T_g(L/2 + L_u) = T_c$. Appropriate expressions for the specular view factors, assuming the exponential kernel approximation are given by Hollands and Iynkaran (1993). We give here only the expression for $dF_{dw-dw'}(z, z')$:

$$dF_{dw-dw'}(z, z') = (c/D) \cdot \exp(-b(z - z')/D) dz' \quad (12)$$

where parameters b and c can be expressed in terms ε_w of the ratio L/D : $b = b(\varepsilon_w, L/D)$ and $c = c(\varepsilon_w, L/D)$, the necessary expressions having been given by Hollands et al. (1984). Expressions for the other specular view factor can be derived from Eq. (12), using flux algebra. Details are given by Hollands et al. (1984) and Youngberg (2000).

To commence the solution of this set of equations, one starts by substituting Eq. (4) for J_{pu} into Eqs. (3) and (5) for J_{pl} into Eq. (7), and then dropping Eqs. (4) and (5) from the set. The number of equations is thereby reduced by two, as is the number of variables, since J_{pu} and J_{pl} are thereby eliminated. Compared to the system of equations in the treatment by Hollands and Iynkaran (1993), the present set has one more variable, namely the temperature of the greenhouse plastic, T_p and one more equation, namely Eq. (9). Other than this the equations are very similar and their solution procedure can be readily extended to the present case. Thus we do not give details; we simply give a summary. Interested readers are referred to Youngberg (2000) for the details.

First the system of equations is de-dimensionalized, in the process introducing the dimensionless counterpart of T_p , which is defined as $\gamma_7 = (T_p^4 - T_c^4)/(T_h^4 - T_c^4)$. At the same time the meaning of γ_7 and γ_8 in the Hollands and Iynkaran treatment is changed to that of γ_8 and γ_9 in the present treatment. All other γ s have the same meaning as they had in that earlier study. Upon following the same steps as in the Hollands and Iynkaran treatment, the problem is reduced to finding the solution to the matrix equation:

$$\mathbf{U} \cdot \mathbf{\Gamma} = \mathbf{V} \quad (13)$$

where $\mathbf{\Gamma}$ is the column vector with elements $(\gamma_1, \gamma_2, \gamma_3, \dots, \gamma_8, \gamma_9)$, \mathbf{U} is a 9×9 matrix and \mathbf{V} is a 9-element column vector. \mathbf{U} and \mathbf{V} are functions of the parameters of the problem, which are T_h , T_c , the radiant properties, D , L , t , L_u , k_c , k_g , h_1 , and the exponential kernel fitting parameter b and c . The elements u_{ij} of \mathbf{U} and v_i of vector \mathbf{V} are either equal to zero or given in terms of these parameters, as follows:

$$\begin{aligned}
 u_{11} &= 1, & u_{12} &= v_1, & u_{13} &= -\omega_2\varphi_1, \\
 u_{14} &= \omega_1\varphi_2, & u_{16} &= -1, & u_{21} &= (1 - \Omega_3\lambda), \\
 u_{22} &= (-v_1\Omega_3(v_1\lambda - 2\mu)), \\
 u_{23} &= (\omega_1\varphi_2 - \Omega_3\omega_2(\varphi_3\lambda\varphi_1)), \\
 u_{24} &= (-\omega_2\varphi_1 - \Omega_3\omega_1(\varphi_3 + \lambda\varphi_2)), \\
 u_{25} &= -\tau_p, & u_{26} &= -\Omega_3(c - \lambda), & u_{27} &= -\varepsilon_p, \\
 u_{31} &= 1, & u_{32} &= -\mu, & u_{33} &= \varphi_2, & u_{34} &= \varphi_1, \\
 u_{37} &= -1, & u_{41} &= 1, & u_{42} &= \mu, & u_{43} &= \varphi_1, \\
 u_{44} &= \varphi_2, & u_{48} &= -1, & u_{49} &= -\mu, & u_{58} &= 1, \\
 u_{59} &= (L_u/D + \mu), & u_{61} &= (\tau_p\lambda\Omega_1), \\
 u_{62} &= (\tau_p\Omega_1(v_1\lambda - 2\mu)), & u_{63} &= (\Omega_1\omega_2\tau_p(\varphi_3 - \lambda\varphi_1)), \\
 u_{64} &= (\Omega_1\omega_1\tau_p(\varphi_3 + \lambda\varphi_2)), & u_{65} &= ((1 - \varepsilon_h)\rho_p - 1), \\
 u_{66} &= (\Omega_1\tau_p(c - \lambda)), & u_{67} &= ((1 - \varepsilon_h)\varepsilon_p), \\
 u_{71} &= (\lambda\Omega_2(\kappa + 1)), & u_{72} &= (\Omega_2(v_1\lambda - 2\mu)(\kappa - 1)), \\
 u_{73} &= (\Omega_2(\kappa\omega_2(\varphi_3 - \lambda\varphi_1) + \omega_1(\varphi_3 + \lambda\varphi_2))), \\
 u_{74} &= (\Omega_2(\kappa\omega_1(\varphi_3 + \lambda\varphi_2) + \omega_2(\varphi_3 - \lambda\varphi_1))), \\
 u_{75} &= (\Omega_2\tau_p(c - \lambda)), & u_{76} &= (-1 + \Omega_2\kappa(c - \lambda)), \\
 u_{77} &= (\Omega_2\varepsilon_p(c - \lambda)), & u_{81} &= (-\lambda/c), \\
 u_{82} &= (-(1/c)(v_1\lambda - 2\mu) - (k_c/(h_rD))), \\
 u_{83} &= ((-\omega_2/c)(\varphi_3 - \lambda\varphi_1) - (k_cP\varphi_2)/(h_rD)), \\
 u_{84} &= ((-\omega_1/c)(\varphi_3 + \lambda\varphi_2) + (k_cP\varphi_1)/(h_rD)), \\
 u_{85} &= -1, & u_{86} &= -(c - \lambda)/c, & u_{87} &= (2 + h_1h_r), \\
 u_{91}W' &, & u_{92} &= (1 + W'\mu), & u_{93} &= (W' + P\varphi_1), \\
 u_{94} &= (W' - P)\varphi_2, & u_{96} &= -W', & u_{99} &= -(h_uL_uk_c), \\
 v_1 &= -Y_c, & v_2 &= Y_c(\varepsilon_p - 1 + \Omega_3\lambda), \\
 v_6 &= -\varepsilon_hY_h - (1 - \varepsilon_h)\varepsilon_pY_c - \tau_p\lambda\Omega_1Y_c, \\
 v_7 &= -Y_c(\varepsilon_c\Omega_2\varepsilon_p(c - \lambda) + \Omega_2\lambda(\kappa + 1)), \\
 v_8 &= -2Y_cY_c\lambda/ch_1h_r, & v_9 &= -W'Y_c
 \end{aligned} \tag{14}$$

These expressions contain some new quantities (such as λ , W etc.). These are defined in the nomenclature.

2.4. Obtaining the heat transfer

Eq. (13) can be solved by standard matrix inversion algorithms, once the parameters have all be determined. But two of the parameters are unknown at the beginning of the solution procedure: h_1 and $k_g = h_uL_u$, since these convective coefficients are functions of the temperatures bounding the two layers. While two of these temperatures, T_h and T_c are known from the start, T_p and $T_w(L/2)$ are not. Consequently, a trial and error iteration must be entered into: in the first step T_p and $T_w(L/2)$ are guessed; then (step 2) h_1 and k_g are calculated, permitting the determination of \mathbf{U} and \mathbf{V} . Then is determined through matrix inversion. This permits the determination of new values of T_p and $T_w(L/2)$. These latter values provide improved guesses for returning to the step 2 for the next iteration. The process is repeated

until T_p and $T_w(L/2)$ change by less than some small amount—like 0.001 K—from one iteration to the next.

Once a solution for Γ is found, the total heat transfer coefficient, $h_t = q/(T_h - T_c)$, where q is the heat flux carried from the hot plate to the cold plate, can be found by evaluating the heat flux at the hot plate, yielding

$$h_t = h_1(1 - \gamma_7) + \frac{\varepsilon_h\sigma}{1 - \varepsilon_h} \cdot \frac{T_h^4 - \gamma_5(T_h^4 - T_c^4)}{T_h - T_c} \tag{15}$$

The heat transfer coefficients h_1 and h_u are determined from the appropriate equation for the heat transfer across a gas layer heated from below. In this study, the equation due to Hollands et al. (1976) was applied.

To test its consistency, the model was compared to the model of Hollands and Iynkaran (1993) in predictions of the heat transfer across regular and compound honeycombs. As expected, since the basis of the models is the same, the predictions were essentially the same (i.e., the same to within 0.05%).

3. Experiment

3.1. Overview

To test the model, values of h_t were measured on a set of honeycombs, and the results compared to the predictions of the model. The nine honeycombs tested were provided by Advanced Glazings Ltd., Sydney, Nova Scotia. These test honeycombs all had nominally square cells of nominal size 10×10 mm and all were made of UV-stabilized polypropylene. They had, on the other hand, varying depths, L , and wall thickness $2t$. There were three thicknesses: $2t = 25, 51, \text{ and } 76$ μm , respectively; and three depths: $L = 45, 64, \text{ and } 76$ mm, respectively, and the nine honeycomb samples included all possible combinations of L and t . Each of these honeycombs was tested while resting on one of two greenhouse polyethylene sheets, both sheets having been especially designed for use in greenhouses. One sheet was “standard stock” and the other had been treated to give it a higher emissivity, enhancing its ability to shield radiation from the greenhouse floor. Of the 18 available combinations of honeycomb and greenhouse plastic, a subset of nine was chosen for the measurements.

3.2. Radiant properties of honeycomb film and greenhouse plastic

The thermal properties of the honeycomb film and greenhouse plastic film needed to be determined for input into the model. The method used was that described in Hollands et al. (1984). Thus, an infrared reflectometer (Gier-Dunkle DB100) was used to measure the infrared reflectance of the film with the black reference behind it.

Table 1
Hemispheric Radiant Properties of Films Used in Experiments

	ρ_w or ρ_p	τ_w or τ_p	ε_w or ε_p
25 μm polypropylene honeycomb wall	0.129	0.807	0.063
51 μm polypropylene honeycomb wall	0.131	0.770	0.100
76 μm polypropylene honeycomb wall	0.132	0.726	0.142
Regular greenhouse plastic sheet	0.099	0.613	0.288
High- ε greenhouse plastic sheet	0.150	0.376	0.474

Then this measurement was repeated with the gold reference behind the film. The infrared reflectance and transmittance of the film itself were then calculated from these values, using equations given by Hollands et al. These measured values were the normal values—i.e., those for the incident radiation perpendicular to the film. These values were converted to their hemispherical counterparts, using a theoretical model similar to that of Hollands and Wright (1983). The results are shown in Table 1.

3.3. Heat transfer measurements

The heat transfer experiments were carried out using the Guarded Heater Plate Apparatus (GHPA), built originally for basic natural convection studies (El-Shirbiny et al., 1982) and later for window studies (Wright and Sullivan, 1988). In the present work, this apparatus was adapted to measure the total heat transfer coefficient, h_t , across the double compound honeycomb configuration shown in Fig. 1b. The GHPA has two parallel main copper plates, one hot and one cold, which were kept horizontal in the present experiments. The hot plate has a set of central guarded heater plates imbedded in it. A support frame keeps the items in place. The maximum attainable plate spacing available on the GHPA was 450 mm. The temperature of each of the $635 \times 635 \times 12.7$ mm ($25 \times 25 \times 0.5$ in.) main copper plates is independently controlled. A temperature-regulated water–glycol solution flows through a manifold soldered to the back face of each plate. Heat transfer measurements are made possible through the use of the guarded heater plate setup, which contained a heat flux meter as well as an electrically heated copper plate. Additional instrumentation included a thermocouple to measure the temperature of the hot plate and six thermocouples connected in series (forming a thermopile) to measure the temperature difference across the plates.

The apparatus was configured to represent the model shown in Fig. 1b, as closely as possible. The

faces of the main copper plates were painted black to achieve a measured plate emissivity of 0.96 ± 0.005 . Supporting the cold plate and also forming the side-walls of the testing enclosure were reflective foil-covered sections of 25 mm thick polystyrene foam insulating boards. The enclosure was sealed and enclosed with fibreglass to minimize air infiltration and heat loss to the environment. The honeycomb samples were mounted in a foil-wrapped frame and rested on a taut piece of greenhouse plastic. The lower plate temperature was set to 20 °C and the upper at 0 °C for all the measurements. The gaps above and below the honeycomb were set so as to make L_u and L_l both equal to 170 mm. These settings achieved the highest Rayleigh numbers possible for the rig without introducing significant edge effects in the radiative and convective heat transfer modes. The calculated Rayleigh numbers in the gaps ranged from 1.5×10^6 to 4×10^6 ; in this range, h_u and h_l are very nearly independent of the gap-spacings. Thus, although the gap-spacings in the experiment were much smaller than those in the greenhouse, the experimental heat transfer coefficients will nonetheless be quite representative of those experienced in a greenhouse.

The temperature baths were run for about 2 h until the plates reached steady-state temperatures. After each adjustment to the input voltage of the resistance heater, the apparatus was left for about 30 min to allow it to reach a new steady state. Steady-state voltages from the heat flux meter were recorded for each resistance heater input value. These adjustments and readings continued until the heat flux meter was as close as possible to a zero reading. An error analysis showed that the random error was $\pm 0.07 \text{ W m}^{-2} \text{ K}^{-1}$ and the bias error was $0.33 \text{ W m}^{-2} \text{ K}^{-1}$. The main contributor to the bias error was the edge effects having to do with the fact that the plates were of a finite size and did not achieve the infinite size assumed in the model.

Plotted in Fig. 3, the measured values of h_t were found to range from 2.48 to $3.13 \text{ W m}^{-2} \text{ K}^{-1}$ for the honeycombs resting on the regular greenhouse plastic and from 2.19 to $2.72 \text{ W m}^{-2} \text{ K}^{-1}$ for the honeycombs resting on the low-emissivity greenhouse plastic. There is a definite and consistent trend in the data toward lower values of h_t when L is increased, or t is increased, or both are increased.

4. Comparison of model and measurements

Fig. 3 shows a plot of all the results by plotting the value of h_t predicted by the model against the measured value. The model is seen to consistently over-predict the measured results, as the predicted results range from 7.3% to 16.3% above the measured results. Some of this error can be attributed to the side-effects, i.e.,

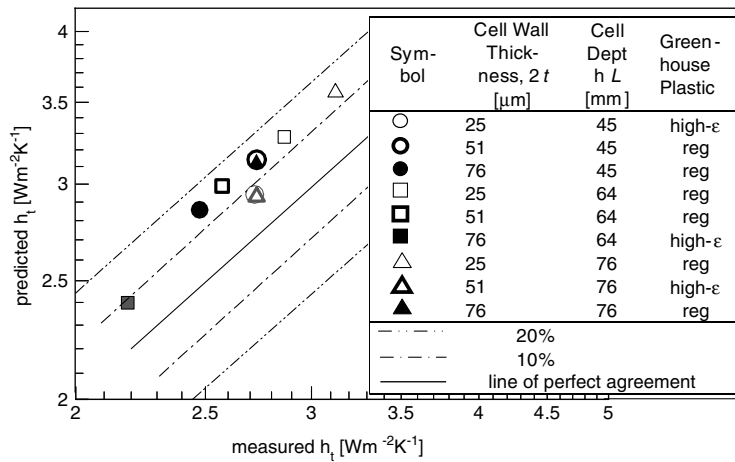


Fig. 3. Comparison between model predictions and experimental results.

the finite horizontal extent of the cavities above and below the honeycomb. Another likely source of error is the assumption that the honeycomb cell walls reflected and transmitted long-wave radiation in a specular manner. This assumption would result in the actual heat transfer being under-predicted by the model, as was observed. The smallest relative errors were observed in runs with the high emissivity greenhouse plastic. This trend may indicate that high emissivity greenhouse plastic conformed more closely than the regular greenhouse plastic to the assumption of a diffuse plastic sheet. Also a possible contributor is the estimation of h_u , which was estimated from a correlation equation that was based on solid boundaries for the air layer, whereas the actual boundary is the face of a honeycomb.

5. Conclusions

While not fully predictive, the model is considered to be accurate enough for design purposes. With the model at hand, the suitability of various combinations of greenhouse plastic and honeycomb designs can be assessed. It should be noted that the model predicts a heat transfer coefficient of $4.25 \text{ W m}^{-2} \text{ K}^{-1}$ when there is no honeycomb present and the regular greenhouse plastic is used and $3.65 \text{ W m}^{-2} \text{ K}^{-1}$ when there is no honeycomb present and the high-emissivity greenhouse plastic is used. This means the reduction in the overall heat transfer coefficient afforded by adding the present design of honeycomb ranges up to 39% reductions.

References

Arulanantham, M., Kaushika, N.D., 1996. Coupled radiative and conductive thermal transfers across transparent insulation materials. *Appl. Thermal Eng.* 16 (3), 209–217.

ElShirbiny, S.M., Raithby, G.D., Hollands, K.G.T., 1982. Heat transfer by natural convection across vertical and inclined air layers. *J. Heat Transfer* 104, 96–102.

Hollands, K.G.T., Iynkaran, K., 1984. Proposal for a compound honeycomb collector. *Solar Energy* 35, 309–316.

Hollands, K.G.Y., Iynkaran, K., 1993. Analytical model for the thermal conductance of compound honeycomb transparent insulation, with experimental validation. *Solar Energy* 51 (3), 223–227.

Hollands, K.G.T., Raithby, G.D., Russell, F.B., Wilkinson, R.G., 1984. Coupled radiative and conductive heat transfer across honeycomb panels and through single cells. *Int. J. Heat Mass Transfer* 7 (11), 2119–2131.

Hollands, K.G.T., Unny, T.E., Raithby, G.D., 1976. Free convection heat transfer across inclined air layers. *J. Heat Transfer* 98, 189–193.

Hollands, K.G.T., Wright, J.L., 1983. Heat loss coefficients and effective $\tau\alpha$ products for flat plate collectors with diathermic covers. *Solar Energy* 30, 211–216.

Hollands, K.G.T., Wright, J.L., Granqvist, C., 2001. Glazings and coatings. In: Gordon, J.M. (Ed.), *Solar Energy: A Century of Progress*. James and James, London, UK.

Platzer, W.J., 1992. Total heat transport data for plastic honeycomb type structures. *Solar Energy* 49 (5), 351–358.

Wright, J.L., Sullivan, H.F., 1988. Glazing system U-value measurement using a guarded heat-plate apparatus ASH-RAE Trans. 4(2).

Youngberg, J.E., 2000. Solar transmittance and heat transfer through polypropylene honeycombs in a greenhouse. M.Sc. Thesis. Department of Mechanical Engineering, University of Waterloo, Waterloo, Ont., Canada.